AGU PUBLICATIONS

Water Resources Research

RESEARCH ARTICLE
10.1002/2013WR015111

Key Points:
- Quantitative connection between CTRW parameters and conductivities is determined
- Dynamic controls are critical factors to determine key transport features
- Transport is not explained only by structural knowledge of the disordered medium

Correspondence to:
B. Berkowitz,
brian.berkowitz@weizmann.ac.il

Citation:
Edery, Y., A. Guadagnini, H. Scher, and B. Berkowitz (2014), Origins of anomalous transport in heterogeneous media: Structural and dynamic controls, *Water Resour. Res.*, *50*, 1490–1505, doi:10.1002/2013WR015111.

Received 27 NOV 2013
Accepted 28 JAN 2014
Accepted article online 3 FEB 2014
Published online 22 FEB 2014

Origins of anomalous transport in heterogeneous media: Structural and dynamic controls

Yaniv Edery[1], Alberto Guadagnini[2,3], Harvey Scher[1], and Brian Berkowitz[1]

[1]Department of Earth and Planetary Sciences, Weizmann Institute of Science, Rehovot, Israel, [2]Dipartimento di Ingegneria Civile e Ambientale, Politecnico di Milano, Milano, Italy, [3]Department of Hydrology and Water Resources, University of Arizona, Tucson, Arizona, USA

Abstract Anomalous (or "non-Fickian") transport is ubiquitous in the context of tracer migration in geological formations. We quantitatively identify the origin of anomalous transport in a representative model of a heterogeneous porous medium under uniform (in the mean) flow conditions; we focus on anomalous transport which arises in the complex flow patterns of lognormally distributed hydraulic conductivity (K) fields, with several decades of K values. Transport in the domains is determined by a particle tracking technique and characterized by breakthrough curves (BTCs). The BTC averaged over multiple realizations demonstrates anomalous transport in all cases, which is accounted for entirely by a power law distribution $\sim t^{-1-\beta}$ of local transition times. The latter is contained in the probability density function $\psi(t)$ of transition times, embedded in the framework of a continuous time random walk (CTRW). A unique feature of our analysis is the derivation of $\psi(t)$ as a function of parameters quantifying the heterogeneity of the domain. In this context, we first establish the dominance of preferential pathways across each domain, and characterize the statistics of these pathways by forming a particle-visitation weighted histogram, $\mathcal{H}_w(K)$, of the hydraulic conductivity. By converting the ln(K) dependence of $\mathcal{H}_w(K)$ into time, we demonstrate the equivalence of $\mathcal{H}_w(K)$ and $\psi(t)$, and delineate the region of $\mathcal{H}_w(K)$ that forms the power law of $\psi(t)$. This thus defines the origin of anomalous transport. Analysis of the preferential pathways clearly demonstrates the limitations of critical path analysis and percolation theory as a basis for determining the origin of anomalous transport. Furthermore, we derive an expression defining the power law exponent β in terms of the $\mathcal{H}_w(K)$ parameters. The equivalence between $\mathcal{H}_w(K)$ and $\psi(t)$ is a remarkable result, particularly given the nature of the K heterogeneity, the complexity of the flow field within each realization, and the statistics of the particle transitions.

1. Introduction

The transport of dissolved chemicals ("tracers," "particles") in water-saturated geological formations has been the subject of intense study for several decades. While many efforts to quantify patterns of migration and dispersion still employ Fickian-based advection-dispersion models, it is now recognized that anomalous (or "non-Fickian") transport is ubiquitous in the context of chemical transport in porous and fractured geological formations, and needs to be incorporated in both deterministic and stochastic modeling efforts. Literature that addresses theoretical and numerical modeling approaches and experimental evidence of such a behavior is extensive [e.g., *Cushman and Ginn*, 1993; *Berkowitz and Scher*, 1997; *Dagan and Neuman*, 1997; *Haggerty et al*., 2000; *Cirpka and Kitanidis*, 2000; *Cirpka and Surabhin*, 2004; *Sanchez-Vila and Carrera*, 2004; *Berkowitz et al*., 2006; *Morales Casique et al*., 2006a, 2006b; *Le Borgne et al*., 2008; *Willmann et al*., 2008; *Kang et al*., 2011; *Rubin et al*., 2012, and references therein, to mention only a few].

Anomalous transport manifests itself in different forms, most commonly appearing as long tails in the spatial and/or temporal distributions of solute concentration (or particles) at given locations. These long tails are typical of solute breakthrough curves (BTCs), which are observed as integral measures along a crossing surface or a monitoring borehole in the domain. This tailing is typically interpreted as a result of spreading, which can in turn be associated with effects of medium heterogeneity exhibited at multiple scales. Theoretical and numerical studies have attempted to explore the origin of this behavior and quantify the effect of the underlying heterogeneous structure of the hydraulic conductivity (K) distribution on such manifestation of solute dynamics.

1.1. Modeling Anomalous Transport

Different modeling strategies could in principle be employed to quantify anomalous transport at the scales where a porous medium is typically treated as a continuum system. In the present work, we focus on two well-established approaches, one using theory and the other based on simulations and analysis of preferential pathways, and unite them. The theory employs the continuous time random walk (CTRW) framework. It has been shown to offer a remarkably flexible interpretation and prediction of laboratory and field scale transport settings [e.g., *Berkowitz et al*., 2006; *Ciriello et al*., 2013, and references therein]. A synthesis of the key features and parameters involved in the CTRW formulation is presented in section 2. The parameters in the governing CTRW transport equation have been related, at least partially, to physical and statistical measures characterizing geological materials [e.g., *Bijeljic and Blunt*, 2006; *Berkowitz and Scher*, 2009].

Dispersion, which results in solute spreading at the scale of observation, is accounted for entirely by a power-law distribution of local transition times, defined within a probability density function (pdf) $\psi(t)$, which is at the core of CTRW. The same quality of CTRW analysis has been manifested in quite a variety of studies of BTCs [e.g., *Berkowitz et al*., 2000; *Kosakowski et al*., 2001; *Bromly and Hinz*, 2004; *Cortis et al*., 2004; *Kosakowski*, 2004; *Bijeljic and Blunt*, 2006; *Mettier et al*., 2006; *Berkowitz et al*., 2008; *Berkowitz and Scher*, 2009; *Bijeljic et al*., 2011; *Kuntz et al*., 2011; *Rubin et al*., 2012]. Moreover, direct measurements of plume propagation in a highly anomalous range [*Bijeljic et al*., 2013a, 2013b] display a form that has been determined by CTRW [*Montroll and Scher*, 1973; *Margolin and Berkowitz*, 2002].

The $\psi(t)$ features a truncation to the power-law distribution (TPL), which introduces the role of the residence time. Evidence that solute residence time exerts a key influence on macroscale transport behavior is provided by *Berkowitz and Scher* [2009]. These authors model BTCs observed during laboratory-scale experiments performed on the same porous medium at three different flow rates. They employ a TPL with a single set of parameter values. Previous interpretations [*Levy and Berkowitz*, 2003] that fit the BTCs with velocity dependent parameters were shown in *Berkowitz and Scher* [2009] to be a consequence of the shift in the experimental duration time relative to the truncation time of the $\psi(t)$. Hence, possibly expecting a rigid slide of the BTCs along the time axis, one instead encounters a change in shape of the BTCs due to the change in velocity. This result allows further exploration of subtle effects of the complete form of $\psi(t)$. The truncation time, which denotes the transition to Fickian behavior, is virtually impossible to assess only on the basis of knowledge of the medium hydraulic conductivity distribution.

The numerically determined $\psi(t)$ from tracer movement, via particle tracking in a pore network model, has been used to obtain the scaling of the longitudinal dispersion coefficient D_L with Péclet number, in agreement with Darcy scale experimental measurements [*Bijeljic and Blunt*, 2006]. Such results using CTRW have been based on a small number of parameters, mainly β and t_2 (see section 2). The main challenge now is to relate these parameters to the source of medium heterogeneity at the scale of interest. More specifically, here, we examine particle path statistics in a model conductivity field and establish these relationships between $\psi(t)$ and subtle features of particle-weighted preferential pathways.

1.2. Conductivity Fields and Preferential Pathways

The general study of conductivity fields and preferential pathways is quite extensive. We discuss these studies in terms of the features that have been learned and what has emerged. A key goal is the understanding of the interplay between the correlation structure of the conductivity and velocity fields and their interaction on the features of anomalous transport behavior observed at the continuum scale [e.g., *Le Borgne et al*., 2008; *Berkowitz and Scher*, 2010]. While equations relating velocity correlation parameters to statistical moments of K are available, the link between these quantities is generally not explicit [e.g., *Tartakovsky and Neuman*, 1998; *Guadagnini and Neuman*, 1999; *Rubin*, 2003; *Panzeri et al*., 2013, and references therein, to mention only a few].

It is difficult to determine a priori solute/particle preferential pathways relying only on information on the K distribution and it is virtually impossible to know if the domain regions associated with the lowest K values are even interrogated or recognized during particle transport without solving the flow and transport problem. Representative values of hydraulic conductivity are known to depend not only on the statistical properties of the underlying conductivity field but also on the type of flow regime occurring in the system, as driven by boundary conditions and source terms [*Sanchez-Vila et al*., 2006, and references therein]. Given the generally (space-time) nonlocal nature of transport at the continuum scale, all length scales over which

aquifer heterogeneities are distributed need to be taken into account to provide prediction of solute distribution at a desired process scale together with the associated uncertainty.

The occurrence of preferential pathways in stationary conductivity fields has been shown by, e.g., *Cirpka and Kitanidis* [2000] and *Willmann et al*. [2008]: these pathways are not apparent by analyzing only the conductivity distribution but can be seen clearly in terms of distributions of velocity and solute plumes traveling through the velocity fields. Under these conditions, modification of a mean uniform hydraulic gradient acting on the system does not alter the flow lines, but the residence time, and thus the possibility of particles to interrogate low-conductivity regions through the effect of diffusion or local dispersivity, can be severely affected.

In this context, it has been noted that Lagrangian velocity correlations are relevant in controlling solute dynamics along flow paths [*Berkowitz and Scher*, 1998; *Le Borgne et al*., 2008; *Moroni and Cushman*, 2010, and references therein]. This suggests the possibility of directly relating the origin of manifestations of anomalous transport, as embodied in long-tailed BTCs, to statistical parameters describing the heterogeneity of hydraulic conductivity, upon which velocity correlation ultimately depends.

1.3. Tailing of BTCs

It has been shown numerically that the occurrence of connected high-conductivity paths produces large variations in fluid velocity and significant tailing of solute BTCs. *Zinn and Harvey* [2003], for example, associate the latter with mass transfer between less and more mobile regions, and conclude that tailing may occur in univariate log-Gaussian conductivity fields when conductivity variability is sufficient. *Knudby and Carrera* [2005] provide some insights on the relationship between main features of solute transport and structural properties of the medium through the concept of connectivity indicators. As a key flow connectivity indicator, which depends solely on the spatial distribution of hydraulic conductivity, these authors consider the ratio between the critical path conductivity, K_C, to the spatial geometric mean conductivity of the system, K_C being defined as the lowest value of conductivity along the critical path which is associated with the highest value of minimum conductivity [*Ambegaokar et al*., 1971] (see section 1.4). Their numerical results suggest that flow connectivity and transport indicators (the latter based on the ratio between the average and early solute arrival times) enable identification of the connected paths in the system. The concept of connectivity has also been explored in the context of multipoint geostatistics [e.g., *Strebelle*, 2002; *Huysmans and Dassargues*, 2009; *Mariethoz and Renard*, 2010], but has not been linked in a clear and quantitative manner to the features of transport typically observed in BTCs.

Willmann et al. [2008] use numerical investigations in two-dimensional random realizations of hydraulic conductivity fields, under uniform (in the mean) flow, to explore conditions under which heterogeneity leads to the power law tailing (non-Fickian behavior) observed in solute cross-sectional BTCs. These authors conclude that the origin of such behavior lies in the preferential flow paths that form, as evidenced in the spatial distributions of concentration calculated within (statistically) nonstationary fields. Their results suggest that the slope of the BTC observed within a single realization is insensitive to the (single realization, spatial) variance of the conductivity field and depends on the connectivity of the system. On the other hand, the conductivity variance influences the duration of the time interval within which the tailing behavior is visible. Such behavior can be captured by effective one-dimensional models based on mass transfer between mobile and immobile regions with memory functions. No theoretical or empirical relationships are provided to quantify the dependence of effective parameters appearing in the memory function on heterogeneity parameters (that can be inferred from measurements of hydraulic conductivity).

Tailing observed in cross-sectional or depth-averaged BTCs is shown to be reproducible in a Monte Carlo (statistical) sense through an ADE-based formulation on the basis of a detailed knowledge of the geostatistical description of the spatial variability of hydrofacies distribution and associated attributes (hydraulic conductivity and porosity) under diverse field settings [e.g., *Salamon et al*., 2007; *Llopis-Albert and Capilla*, 2009; *Riva et al*., 2008, 2010].

1.4. Particle Tracking and Critical Path Analysis

Bianchi et al. [2011] investigate the relationship between connectivity and the occurrence of preferential flow paths at the MADE site. Similarly to *Riva et al*. [2008, 2010], they start from core-scale estimates of hydraulic conductivity based on particle size analysis curves and generate three-dimensional (conditional)

realizations of conductivity fields by means of diverse geostatistical methods. Flow and transport (using particle tracking) are then simulated under permeameter-like conditions. Their numerical results show that the first 5% of particles which arrive at the downstream domain boundary (or crossing-plane) are transported through preferential flow paths which carry a significant fraction (about 40%) of the flow. A similar observation was made by *Fiori and Jankovic* [2012] who point out difficulties associated with obtaining field-scale concentration measurements because there is a small probability that solute particles visit highly conductive blocks, especially in the presence of large conductivity variance. *Bianchi et al.* [2011] observe that the fraction of particle paths falling within the high-conductivity regions ranges between 43% and 69% in their simulations. Some of their simulated fastest paths occur through regions with low-conductivity values, suggesting that transport connectivity may not require fully connected zones of relatively homogeneous conductivity.

The analysis of preferential flow paths in heterogeneous media has also been performed through critical path analysis [*Ambegaokar et al*., 1971; *Kirkpatrick*, 1971]. The latter has been linked, using percolation theory scaling arguments, to anomalous transport and CTRW theory [*Hunt et al*., 2011; *Ghanbarian-Alavijeh et al*., 2012; *Sahimi*, 2012]. These studies suggest parameter values that can be used in CTRW formulations, which can then be employed to interpret laboratory and field observations.

1.5. Origins of Anomalous Transport

In this work, we focus on improving our understanding of the nature and key driver of non-Fickian transport in randomly heterogeneous porous media. In this context, we explore by way of a suite of numerical simulations the correspondence between quantitative metrics associated with such fields and parameters embedded in the CTRW formulation. We show that these parameters can be interpreted as identifiable parameters that can be estimated from measurements, with clear and profound physical meaning. Our simulations consider spatially correlated hydraulic conductivity and velocity fields, their impact on non-Fickian transport, and the way their key features can be incorporated within the CTRW formulation.

More specifically, we consider two-dimensional, fluid-saturated domains, generated from a lognormally distributed and spatially correlated hydraulic conductivity random field. The degree of system heterogeneity is quantified by σ^2, the variance of $\ln(K)$. We determine the steady state uniform (in the mean) flow and the transport of tracer particles through the domain, using a standard particle tracking technique. The transport is characterized by BTCs, which quantify the arrival of an injected plume of particles at crossing planes located at two distances from the domain inlet. BTCs obtained as averages over a collection of realizations document anomalous transport. We identify the origins of anomalous transport in such domains, using an analysis of the particle pathway statistics and particle interrogation of the low-conductivity regions. We demonstrate clearly that the transport cannot be explained solely by the structural knowledge of the disordered medium, in terms of the spatial arrangement of hydraulic conductivity blocks. By probing the nuanced dynamic processes, we find that the basic determinant of the distribution of local transition times, $\psi(t)$, which defines the anomalous transport, is a conductivity histogram weighted by the particle flux. Based on the statistical analysis of flux-weighted particle pathways, these findings are then related to geostatistical parameters governing the structure of the hydraulic conductivity field and to CTRW parameters.

Clearly, a very wide range of "permutations and combinations" of geostatistical parameters (e.g., mean and variance of $\ln(K)$, correlation length, anisotropy ratio) and flow conditions (e.g., hydraulic head gradient, boundary conditions, two-dimensional and three-dimensional systems) could be considered; they are linked in multiple, complex ways to the overall transport dynamics and structural aspects. In the current study, we focus on specific parameter combinations that enable us to focus deeply on the underlying dynamics and develop, for the first time, a clear connection between CTRW parameters and physically defined quantities.

Studies of heterogeneous conductivity fields have shown that there are preferential pathways, and that the low-conductivity regions contribute to anomalous transport. We examine these features in detail, so that we can relate quantitative descriptions of BTCs to the interplay of the structure of the conductivity field and the dynamics of the associated flow field. Precisely what is the direct connection between CTRW key parameters and the underlying description of the hydraulic conductivity field and the flow patterns? Can this connection be determined strictly by metrics quantifying the structure of the disordered medium? How does the full range of the low-conductivity regions (including ones that solute particles do not enter) play their role? What is the spatial distribution of these key regions, especially in relation to the preferential pathways?

Are they contained in the preferential pathways? Do these regions account for the power-law in $\psi(t)$? Does the transport homogenize over the medium when it evolves to Fickian behavior and an ADE description? Is critical path analysis a viable link between the heterogeneous structure of the conductivity field and solute transport, as embodied in BTCs? Answering these questions represents our approach to discerning the origin of anomalous transport.

2. The CTRW Framework

We briefly review the basic CTRW formulation as considered in this current study; a detailed exposition of the background and development is given in *Berkowitz et al*. [2006].

The CTRW continuum transport equation for the normalized concentration $c(\mathbf{s}, t)$ for an ensemble-averaged system, in Laplace space, is

$$u\tilde{c}(\mathbf{s},u)-c_0(\mathbf{s})=-\tilde{M}(u)[\mathbf{v}_\psi\cdot\nabla\tilde{c}(\mathbf{s},u)-\mathbf{D}_\psi:\nabla\nabla\tilde{c}(\mathbf{s},u)] \tag{1}$$

where $\tilde{M}(u)\equiv\bar{t}u\tilde{\psi}(u)/[1-\tilde{\psi}(u)]$ is a memory function, $\bar{t}$ is a characteristic time, $\psi(t)$ is the probability rate for a transition time t between sites, and $\bar{t}\mathbf{v}_\psi$ and $\bar{t}\mathbf{D}_\psi$ are, respectively, the first and second moments of $p(\mathbf{s})$, defined as the probability distribution of the length of the transitions (with $\mathbf{s}$ the position vector). The Laplace transform of a function $f(t)$ is denoted by $\tilde{f}(u)$. In contrast to the classical advection-dispersion equation (see below), the "transport velocity," $\mathbf{v}_\psi$, is in principle distinct from the "average fluid velocity," $\mathbf{v}$. Solutions of (1), to analyze solute BTCs, are readily available in *Cortis and Berkowitz* [2005].

A key feature of (1) is the choice of $\psi(t)$. We employ here a functional form that has been particularly successful in interpretations of a number of laboratory and field observations, namely, a truncated power law (TPL) distribution of the site-to-site transition times which enables an evolution to Fickian behavior:

$$\psi(t)=\frac{n}{t_1}\exp(-t/t_2)/(1+t/t_1)^{1+\beta}, \tag{2}$$

where $n\equiv(t_1/t_2)^{-\beta}\exp(-t_1/t_2)/\Gamma(-\beta,t_1/t_2)$ is a normalization factor (for large t_2, $n\approx\beta$, see (37) and Appendix B in *Berkowitz et al*. [2008]) and $\Gamma(a,x)$ is the incomplete Gamma function [*Abramowitz and Stegun*, 1970]. Here we set the characteristic time $\bar{t}$, appearing in (1), equal to t_1; this represents the onset of the power law region. This form of $\psi(t)$ behaves as a power law $\propto(t/t_1)^{-1-\beta}$ for transition times $t_1<t<t_2$. For $t>t_2$, $\psi(t)$ decreases exponentially, so that a finite t_2 enables smooth evolution from non-Fickian to Fickian transport.

Significantly, specifying a pure exponential form $\psi(t)=\lambda\exp(-\lambda t)$ reduces the CTRW transport equation (1) to the advection-dispersion equation (ADE), given in a general form:

$$\partial c(\mathbf{s},t)/\partial t=-\mathbf{v}(\mathbf{s})\cdot\nabla c(\mathbf{s},t)+\nabla\cdot[\mathbf{D}(\mathbf{s})\nabla c(\mathbf{s},t)] \tag{3}$$

where **v(s)** is the velocity field and **D(s)** is the dispersion tensor.

The parameters appearing in $\psi(t)$ can in some cases be derived from the physical structure of the system, i.e., they are more than simple calibration/tuning quantities. The most important of these parameters is β, and physical models exist for its exact determination [*Pfister and Scher*, 1978; *Scher et al*., 1991], as well as for the entire $\psi(t)$ [*Scher and Lax*, 1973]. One prime example is a multiple trapping model in a disordered semiconductor, containing localized energy levels with an exponential distribution $\rho(E)\sim\exp(-E/kT_0)$, where T_0 is the width of the energy distribution in temperature units (k is Boltzmann's constant) and the particle trap release rate has a Boltzmann activation form $W_0\exp(-E/kT)$, where T is the temperature. The exact determination is $\beta=T/T_0$, which has been observed in experimental time-of-flight measurements in amorphous semiconductors, molecularly doped polymers [*Scher et al*., 1991, and references therein]. This result can have general application, e.g., for chemical absorption in a disordered medium, as long as the absorption-site density varies as $\exp(-E/kT_0)$.

Another exact derivation results from an ensemble average that has been obtained for the entire $\psi(t)$ for a particle hopping among a random distribution of sites (the so-called η function) [*Scher and Lax*, 1973]. The

site density controls the disorder. This derivation of $\psi(t)$, from a physical model, has become the prototype form for $\psi(t)$ for disordered systems, clearly showing power-law like behavior for sufficient disorder and a cutoff; e.g., it is the basis for using the TPL (2).

The TPL has been used to determine β and t_2, in conjunction with determination of the distribution of times for, e.g., the North Sea field site [*Di Donato and Blunt*, 2004] and for a pore network model (see *Berkowitz et al*. [2006] for more discussion). For the latter model, t_2 was calculated from LD_m/Pe [*Bijeljic and Blunt*, 2006], where D_m is the molecular diffusion coefficient, L is a characteristic length, and Pe is the Péclet number. To date, it is the only linkage of t_2 to parameters governing physical processes, except for an approximation to the η function.

3. Numerical Methods and Particle Tracking

Our numerical study considers a setting associated with uniform (in the mean) saturated flow within a two-dimensional domain measuring 300×120 (all quantities are expressed in the same space-time units) discretized into grid cells of uniform size $\Delta = 0.2$. Permeameter-like boundary conditions are imposed, with a deterministic head drop ($=100$) across the upstream (left) and downstream (right) boundaries, and no-flow conditions along the two remaining boundaries of the domain. Values of $\ln(K)$ in each cell are set equal to those generated at cell centers through a widely tested sequential Gaussian simulator (GCOSIM3D) [*Gómez-Hernández and Journel*, 1993], with mean $\ln(K) = 0$. We generate random realizations of statistically homogeneous and isotropic Gaussian fields of $\ln(K)$ associated with exponential covariance (see section 4.2 for a typical realization). For this first study, we consider fields associated with a unit correlation length, $\ell = 1$, exploring the impact of different values of the variance of $\ln(K)$, i.e., $3 \leq \sigma^2 \leq 7$, on anomalous solute transport behavior, as manifested in BTCs. As noted by *Fogg* [2010], values even as large as $\sigma^2 = 10$–15 are realistic in natural geological formations. The combination of these values renders log-conductivity fields ranging from mild to strongly heterogeneous conditions (in terms of their variogram sill) and enables us to (a) analyze transport within a region of the domain where the statistics of the underlying velocity field are not significantly influenced by the imposed boundary conditions, as well as (b) consider large solute travel distances relative to the log-conductivity correlation scale. We solve the corresponding deterministic flow problem for each realization of $\ln(K)$ through the code of *Guadagnini and Neuman* [1999] which is based on finite elements with Galerkin weighting functions. We obtain hydraulic head values throughout the domain, which are then converted to local velocities, and thus streamlines. For the system considered here, we used the representative porosity value $\theta = 0.3$ [e.g., *Levy and Berkowitz*, 2003]. A detailed discussion of the connection between correlations in individual realizations, the subsequent ensemble average, and CTRW is given in Appendix A.

On the basis of these calculated streamlines, solute movement in each realization is modeled by a standard Lagrangian particle tracking method, to generate the BTCs [e.g., *Le Borgne et al*., 2008; *Bianchi et al*., 2011]. The selected values of Δ and ℓ assure that $\Delta/\ell < 5.0$ for all scenarios examined, thus rendering an accurate description of small-scale fluctuations of the generated $\ln(K)$ fields and advective transport features [e.g., *Ababou et al*., 1989; *Riva et al*., 2009, and references therein]. Particles are injected along the left boundary, according to flux-weighting, and move by advection and diffusion. The displacement vector $\mathbf{d}$ for each particle is given by the Langevin equation, starting from a known location of the particles at time t_k:

$$\mathbf{d} = \mathbf{v}[\mathbf{x}(t_k)]\delta t + \mathbf{d}_D \tag{4}$$

where $\mathbf{v}$ is the fluid velocity, δt is the time step magnitude, and $\mathbf{d}_D$ denotes the diffusive displacement; ξ is a $N[0, 1]$ random number and the modulus of $\mathbf{d}_D$ is $\xi\sqrt{2D_m\delta t}$. A value of $D_m = 10^{-5}$ cm^2/s was chosen to correspond to the diffusion coefficient of many ions in water [*Domenico and Schwartz*, 1990]. The velocity at $\mathbf{x}$ is used to compute the advective displacement in (4). Local values of velocity are computed upon applying the methodology proposed by *Cordes and Kinzelbach* [1992]. A uniform spatial step, δs, is fixed along each particle trajectory. The magnitude of the time step δt in (4) is calculated as $\delta t = \delta s/v$, v being the modulus of $\mathbf{v}$. Reflection boundary conditions are imposed at no-flow boundaries. Preliminary numerical tests confirmed that consideration of 10^5 particles provided representative results (i.e., simulations were performed by increasing the number of particles tracked up to 10^6 and the results were qualitatively insensitive), and that choosing $\delta s = \Delta/10$ did not introduce significant numerical dispersion.

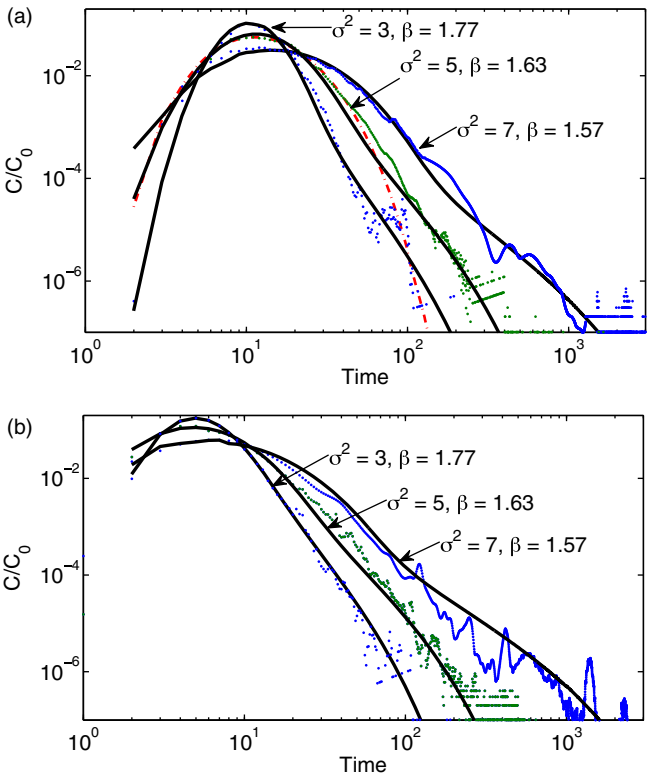

Figure 1. Breakthrough curves (points) for three ln(K) variances ($\sigma^2 = 3,5,7$; 100 realizations each), (a) at the domain outlet ($x = 300$ length units), and (b) at the domain midpoint ($x = 150$ length units), and corresponding CTRW fits (curves), with values of v_ψ, D_ψ, β, t_1, t_2 in (2) of, respectively, [6.0, 15.8, 1.77, 0.055, $10^{1.6}$], [5.5, 46.7, 1.63, 0.04, $10^{2.5}$], [3.8, 60, 1.57, 0.063, $10^{3.0}$]. Also shown in Figure 1a is a fit of the advection-dispersion equation (dashed-dotted curve), for $\sigma^2 = 5$ with $v = 3.4$, $D = 39$. All values are in consistent, arbitrary length, and time units.

Breakthrough curves are determined by generating different realizations of the heterogeneous domain, solving for the fluid flow, and then tracking solute particle migration. The BTCs represent cross-sectional temporal distributions of particles reaching different crossing planes, averaged (cumulative) over 100 realizations. Here BTCs are determined at two distances from the domain inlet, at the domain midpoint and outlet ($x = 150$, 300 length units, respectively), with a head drop across the domain of 100. One hundred simulations were performed for each variance of log hydraulic conductivity; the resulting BTCs were averaged over the collection of realizations. Preliminary numerical simulations confirmed that, in the setting we consider, 100 realizations provide representative average values over a wide range of relative particle concentrations.

4. Results and Discussion

4.1. Breakthrough Curves (BTCs)

We probe transport behavior in heterogeneous systems by first detailing systematics of the overall domain-wide behavior. The BTC curve is a key measure of the cumulative response of all particle transitions that comprise the transport within the domain. The determining "geometric" features are the value of σ^2, which drives the heterogeneity, and the domain length and hydraulic head gradient, which contribute to the residence time. The mean BTCs obtained over 100 realizations are seen in Figure 1a, with $\sigma^2 = 3,5,7$, and fits with 1-D solutions of the CTRW (using (2)) and the ADE. Evaluation of (1) with (2) is detailed in *Berkowitz et al.* [2006]. The distinguishing feature is the broadness of the BTCs, which increases with increasing σ^2. Overall, the CTRW effectively captures the tails as well as the peaks of the BTCs. Here the cutoff time t_2 is established by examining two BTCs (from $x = 150$, 300 length units; see also Figure 1b), to capture the transition from non-Fickian to Fickian transport behavior. We note that the oscillations in the BTC tails are caused by the formation of a limited set of preferential channels (see Figure 2), leading to variations in the distribution of small numbers of particles arriving at the outlet; increasing the number of realizations and/or particles moves the oscillations to even lower relative particle concentrations in the BTC tail.

It is to be emphasized that we are using the BTCs with the CTRW fits here to establish that transport via the flow field in our setting results in anomalous transport. As discussed above there is a large and growing literature demonstrating quantitative accounting for a variety of data sets (e.g., BTCs) with the CTRW framework. A key aspect of the $\psi(t)$ determined in Figure 1 will be its relation directly to the statistics of particle pathways.

The fitted values of β appearing in (2) show a clear trend to decrease (from 1.77 to 1.57) with increasing σ^2 (from 3 to 7), as expected. This emphasizes the physical meaning of β: it is a generalized dispersion parameter that captures the entire shape of the BTC curve and not only a width of a normal curve (i.e., as opposed to, for example, the effect of $\mathbf{D}(\mathbf{s})$ in the ADE (3)). Moreover, as expected, the value of D_ψ increases with increasing σ^2. Below, we quantify the subtle interplay among the parameters β, t_1, and t_2, which determine

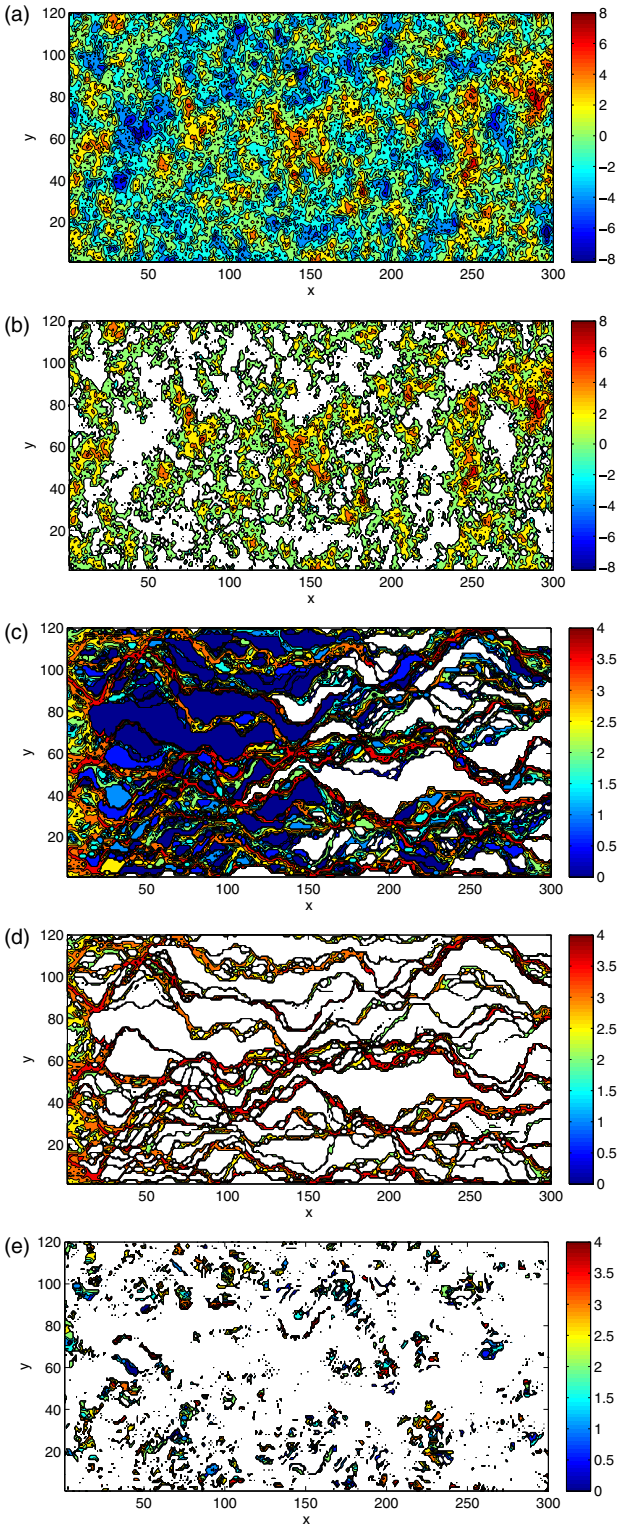

Figure 2. Spatial maps showing (a) full K field, (b) critical path analysis ($\ln(K) < -0.63$), (c) particle paths, (d) preferential particle paths, defined as paths through cells that each contain a visitation of a minimum of 100 particles (= 0.1% of the total number of particles in the domain), (e) "lower conductivity transition jumps" (see text). Note that the color bars are in $\ln(K)$ scale for Figures 2a and 2b, and $\log_{10}$ number of particles for Figures 2c–2e.

the shape of (2), in terms of the particle paths. A ubiquitous feature of transport induced by heterogeneity is a power law that gives the correct weighting of the particle transition times, providing a slowly decreasing access to a wide time base. The tail includes those particles that encounter some relatively lower conductivities. These encounters are less frequent events but have a large effect on the arrival time. An important question is: what part of the conductivity spectrum yields the range $t_1 < t < t_2$?

Note that for the case $\sigma^2 = 5$, the ADE solution deviates significantly from the tail of the BTC. The ADE is fit with two free parameters, namely velocity v and dispersion D. Significantly, the value of $v = 3.4$ for the ADE fit does not correspond well to the mean effective velocity (=1.1, calculated as the ratio between the mean Darcy flux and the porosity), nor to the average fluid velocity $\bar{v}$=5.6 (calculated as the average of the average velocities determined for each particle trajectory), in contrast to the v_ψ values in the CTRW fits. The coincidence with $\bar{v}$ is an important constraint in the fitting parameters, which captures the faster pathways; the contribution to the tail emanates from those particles that encounter relatively lower conductivities (see section 4.2).

In Figure 1b, for the same values of σ^2, we show a comparison between simulations and fitted CTRW BTCs, determined at the midpoint along the domain ($x = 150$ length units); compare to Figure 1a, corresponding to BTCs at the domain outlet ($x = 300$ length units). As before, the fit with a TPL is good. The only change in the TPL fits between these curves is the time (i.e., all of the parameter values v_ψ, D_ψ, t_1, t_2, β are the same). Although the extent of the power law of the TPL does not change (fixed β), the time window sampling the entire shape of the TPL does change. The

larger residence time is closer to the cutoff time t_2. Hence, two different dispersive BTC curves are fit with a single TPL. The fits capture a subtle physical feature of the change in averaging over key particle trajectories with residence time. How this happens will be discussed in section 4.2.

4.2. Path Analysis

In a heterogeneous porous medium, how much of the domain is actually interrogated by tracer particles as they migrate through it? This seemingly innocuous question is key, and turns out to be rather complex. We explore in Figure 2 the statistics of particle pathways. This analysis provides important clues as to how heterogeneity affects transport, more specifically the development of the dynamics of non-Fickian behavior, and the onset of Fickian behavior, as evidenced in the BTCs discussed above.

Figure 2a shows the heterogeneity of the K-field with $\sigma^2 = 5$. The mean ln(K) is 0.26 with a 7 decade spread in K over a statistically homogeneous map of this particular single realization. The lowest values of ln(K) tend to appear as local patches with a concentric region (the size of which is governed by the field correlation scale) of moderately low conductivity. We investigate how this map manifests the preferential pathways of the particles.

As a reference, Figure 2b shows a path constructed by excluding cells where the conductivity is lower than a given threshold; the threshold value is lowered iteratively until a connected (percolation) path is formed. This type of critical path analysis [*Ambegaokar et al*., 1971; *Kirkpatrick*, 1971] has been linked, using percolation theory scaling arguments, to anomalous transport and CTRW theory [*Hunt et al*., 2011; *Ghanbarian-Alavijeh et al*., 2012; *Sahimi*, 2012].

In Figure 2c, we superimpose on the full conductivity field (Figure 2a) the number of particles visiting each cell. The striking feature that emerges is the occurrence of particle preferential pathways from inlet boundary to outlet boundary, which are so dominant that the difference in particle visitation in various cells ranges from 0% to 10% of the total number of particles in the simulation. The white areas in this figure, where particles do not enter, have an effect on the surrounding areas, confining the preferential pathways to converge between low conductivity areas.

Figure 2d shows a sparser set of preferential pathways than Figure 2c, generated by recording only those cells which have been visited by at least 100 particles (i.e., at least 0.1% of all particles). The color contrasts show an admixture of the higher conductivities in the paths, although low conductivity cells are still present in the paths. Significantly, though, the particle flux is not spatially uniform across the domain cross sections, as commonly envisaged for application of the advection-dispersion equation; rather, the flux is still, largely, in limited preferential pathways. As noted in section 1, such behavior was reported by, e.g., *Bianchi et al*. [2011], who found that some of the simulated fastest paths included regions with low conductivity values.

It is illuminating to observe deviations from the particle pathways defined by the critical path analysis. Figure 2e shows the "lower conductivity transitions"—defined for convenience as cells with K values less than the critical path threshold—taken from the paths shown in Figure 2c. Clearly, a critical path analysis is insufficient to predict or estimate the actual particle movement. Indeed, critical path analysis and percolation scaling arguments, based entirely on the K field structure [*Sahimi*, 2012], do not include the significant influence of the transitions below the threshold and residence time effects. It is clear that low K links connect and enhance the number and pattern of preferential pathways, so that, e.g., the tail of the BTC contains the transits of particles through these lower K value regions. Moreover, as we show below, one must incorporate a particle-flux weighting of the K histogram to properly characterize the transport.

Finally, referring again to Figure 2c, and to the BTC fit by the ADE in Figure 1c, the question arises as to how far particles must travel to eventually reach Fickian behavior. The flow becomes increasingly channeled with distance from the inlet, at least over the domain length considered here. While one might expect that the preferential pathways "dissipate" and achieve a more uniform flow pattern at some distance, we note that this does not occur in our simulations. Instead, Fickian transport can arise from particle transport through a limited number of preferential pathways, at long distances/times, and not necessarily because of particle "homogenization" over the entire domain. Rather, the particle flux evolves with distance (or time), and can be envisioned as incorporating a sufficient number of encounters ("statistical homogeneity") to yield a steady, relatively narrow range of dominant velocities (which can be described by a single parameter D). The Fickian limit is reached by the cutoff time t_2. However, in this limit the particle flux is not uniform

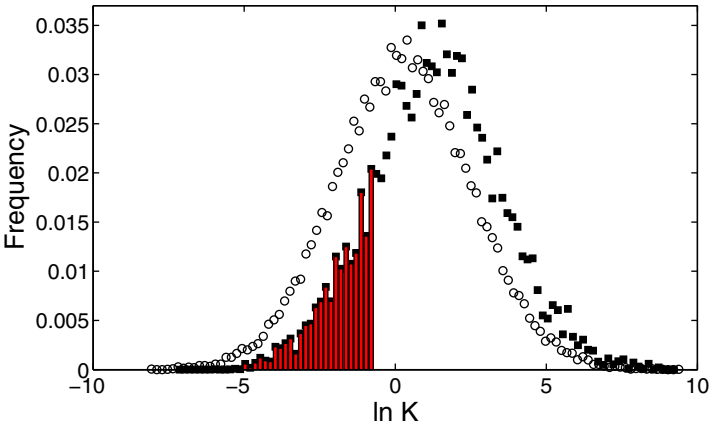

Figure 3. Conductivity histogram normalized by the number of cells (open circles), corresponding to Figure 2a, with mean ln(*K*) of 0.26 and skewness of 0.03. Conductivity histogram of the preferential particle paths (filled squares) (see Figure 2c), weighted and normalized by the number of particles visiting in each conductivity cell, $\mathcal{H}_w(K)$; with weighted mean of 1.43 and skewness is 3.89. Bars (denoted in red) indicate the frequency of lower conductivity transitions (see Figure 2e) in the weighted histogram of the preferential particle paths.

spatially across the domain cross section as commonly envisaged; it is still largely in an augmented preferential pathway region.

4.3. Weighted *K* Histogram and CTRW

Two histograms are shown in Figure 3, together with a quantitative measure of the particle transitions in lower conductivity regions. One histogram corresponds to the conductivity field in Figure 2a, while the other, which we designate $\mathcal{H}_w(K)$, derives from the preferential pathways of Figure 2c weighted by the particle visitation in each cell. Note that $\mathcal{H}_w(K)$ determined from weighted particle visitation only in cells lying within the preferential pathways shown in Figure 2d yields an essentially identical result; only 0.5% of the particles visit cells that do not lie on these preferential pathways. The mean and skewness of the population associated with $\mathcal{H}_w(K)$ are significantly larger than those for the full *K* field (Figure 3). The mean value associated with $\mathcal{H}_w(K)$ is a quantitative measure of the particle selectivity of the higher conductivity cells. The fraction of the weighted conductivities considered as lower conductivity transitions is 16.7%; recall that these transitions lie below the critical path threshold. Hence, these lower conductivity transitions are significant, and as we show below, are responsible for the long tail in the BTC. The $\mathcal{H}_w(K)$ in Figure 3 is obtained from one realization; averaging the weighted mean over 100 realizations for the same σ^2 follows this pattern closely. Moreover, a similar behavior was observed for a variety of realizations with different ln(*K*) variances (see below).

The observed $\mathcal{H}_w(K)$ is the basic characterization of transport in our model. This is seen clearly by converting the ln(*K*) axis to time *t*. Based on Figure 3, for each "*K*-bin" within $\mathcal{H}_w(K)$, we determined the hydraulic head gradient (along the average flow direction) over each associated cell in the flow field, and obtained an average hydraulic head gradient (weighted by the relative number of particles passing through these cells). We then determined the average residence time in these associated cells, using Darcy's law for flow, $\Delta t = \theta(\Delta x)^2/(K^*\Delta h^*)$, where θ is porosity, Δh^* is the weighted average hydraulic head difference, and K^* is the weighted average of the "*K*-bin". Note that modifying the value of θ simply scales Δt. Determining these average times for cells in all *K*-bins, we obtain a frequency (weighted by the number of particles) of particle residence times in all cells in the domain. Dividing by Δt to normalize yields the probability density result for 100 realizations, shown in Figure 4; the entire density is coincident with (2) using $\beta = 1.63$. Significantly, the β, t_1 and t_2 values of (2) used here are the same as those obtained by fitting the BTC in Figure 1 ($\sigma^2 = 5$). Figure 4 is a juxtaposition of this determined $\psi(t)$ and $\mathcal{H}_w(K)$. The statistical analysis of particle paths, which renders the sample probability density $\mathcal{H}_w(K)$, leads directly to the CTRW framework of the probability density $\psi(t)$; indeed, they are the same.

By equating the logarithmic derivatives of both curves, we can develop an analytic expression for β in terms of $\mathcal{H}_w(K)$ parameters. The points in Figure 4 are determined from the numerical $\mathcal{H}_w(K)$ for each realization. The *K* values in Figure 3 are matched by $f = n_k \exp[-(\ln K - \mu)^2/(2\sigma^2)]/t$, where μ is the mean of $\mathcal{H}_w(K)$, and the variance associated with $\mathcal{H}_w(K)$ is $\approx\sigma^2$ (confirmed numerically); n_k is a normalization constant. We compute the logarithmic derivative $d\log f/d\log t$, and obtain (see Appendix B)

$$\beta = (\mu - \ln K)/\sigma^2 \tag{5}$$

by equating it to $-1-\beta$, i.e., to the log derivative of (2). This result has a slow time dependence for β, as can be seen by the slight curvature appearing in the power law region in Figure 4. The value for β is determined near

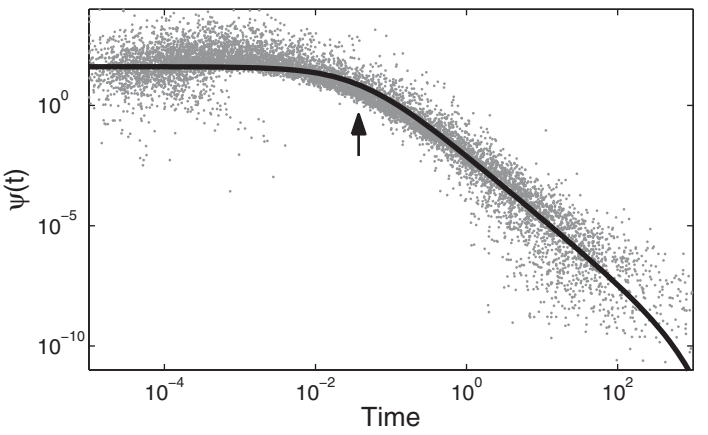

Figure 4. Particle-weighted conductivity histogram ($\sigma^2 = 5$) for 100 realizations (points), based on histograms such as shown in Figure 3, yielding a particle transition time distribution within cells, representing $\psi(t)$ versus t. The solid curve shows (2) with $\beta = 1.63$, $t_1 = 0.04$, and $t_2 = 10^{2.5}$, identical to the values for the fit shown in Figure 1. The arrow is at t_1, the onset of the power law region $t_1 < t < t_2$ corresponding to ln $(K) < -1$. The important part of the juxtaposition is the power law region; the small times $t < t_1$ do not influence the anomalous long-time tailing behavior of the BTCs.

the end of the range of small ln(K) (large time). Using representative ensemble values ($\sigma^2 = 5$, $\mu = 1.5$) and choosing ln(K) $= -6.5$ (the low end (large time) of the lower conductivity transitions in Figure 3) yields $\beta = 1.6$ (see Figure 1). The range of detection for β (the straight line region in Figure 4) is determined between t_1 and t_2, which corresponds to $-6.5 <$ ln(K) < -1 in Figure 3. Furthermore, referring again to Figure 3, note that the range of variance of $\mathcal{H}_w(K)$ is not necessarily identical to that of the entire ln(K); these histograms are plotted on a log scale, for a specific realization, σ^2, and correlation length. The skewness values provide an indication of the true disparity between the two plots.

A picture emerges from the path analysis of high particle flux through the preferential pathways, with encounters of relatively low conductivities (aided by diffusion). The lower conductivity transitions with highest particle flux occur in or near the preferential pathways. The inclusion of these lower conductivity transitions in the context of the preferential pathway template is sufficient to provide to $\mathcal{H}_w(K)$ a power law behavior of $\psi(t)$; this is the origin of non-Fickian transport. It derives from a particular selection of lower conductivity transitions—a reduced part of the spectrum. There is a subtle interplay, where the high-conductivity part of each preferential pathway acts as a funnel into the lower part of the conductivity spectrum. An arrow demarks the start of the power law region $t_1 < t < t_2$ of Figure 4; this region corresponds to a ln(K) range $\lesssim -1$ in the lower conductivity transition region (red bars in Figure 3). The role of the spatial distribution of K is to set up the flow field, which forms the dynamical basis of the preferential pathways. It is the range of lower conductivity transitions within this context that accounts for the anomalous transport, as demonstrated here with the quantitative relation $\mathcal{H}_w(K) \leftrightarrow \psi(t)$. Note also, with regard to critical path analysis, that the power law region lies *below* the critical path threshold. Indeed, many of the lower conductivity transitions are an integral part of the preferential pathways (recall Figure 2e).

5. Summary and Conclusions

We have quantitatively identified the origin of anomalous transport in a representative model of a heterogeneous porous medium. We proceeded via two levels. In the first, we determined the BTCs, which document the anomalous nature of the transport by the power law dependence of late times tails. The BTCs were fit with solutions of the advection-dispersion equation and the CTRW transport equation (1) using the form (2) of $\psi(t)$. The truncated power law accounts for the full shape of the BTCs, with the β parameter decreasing with enhanced disorder (larger σ^2) as expected. This $\psi(t)$ hence serves as a characterization of anomalous transport. The CTRW accounts for (velocity) correlations in *each* realization (recall Appendix A), which leads to a single $\psi(t)$.

In the second level, we examined the nature of the particle pathways across the domain and established the dominance of preferential pathways. We assessed the dynamic statistics of these paths by forming a particle-visitation weighted histogram $\mathcal{H}_w(K)$. We showed that these paths were, mainly, linked high-conductivity cells with an important, sparse mix of a relatively small number of lower conductivity transitions. We converted the ln(K) dependence of $\mathcal{H}_w(K)$ into time and demonstrated the equivalence of $\mathcal{H}_w(K)$ and the $\psi(t)$ in (2). In effect, we show that one can derive (2) directly from the statistical analysis of the actual particle pathways. We further pinpointed the range of the lower conductivity transitions as corresponding to the power law region of (2) and derived a simple expression (5) for β in terms of σ^2 and μ. Thus

all the information associated with transport is contained in $\mathcal{H}_w(K)$—including all correlations in the transitions—and directly yields the values of β as well as t_2 in the CTRW framework. This is a remarkable result, particularly given the nature of the K heterogeneity, the complexity of the flow field within each realization, and the statistics of the particle transitions.

To conclude, the aim of this study was to understand and probe the physical role of different elements in the CTRW equation and the interplay between them and the heterogeneity of the domain (quantified in terms of (statistical) parameters describing the spatial distribution of hydraulic conductivity). The fundamental insights and conclusions of our study are:

- The "origin" of anomalous transport in geophysical and other porous media has been an outstanding question for many years. We develop for the first time a direct connection between CTRW parameters and the randomly heterogeneous hydraulic conductivity field, under uniform (in the mean) flow conditions.
- We show that transport cannot be explained solely by the structural knowledge of the disordered medium (i.e., dynamic/flow controls are critical factors). We point out the critical role of low-conductivity transition zones in controlling transport patterns, and the nature of preferential flow paths.
- We demonstrate that a basic determinant of the distribution of local transition times, which defines the underlying transition time pdf used in the CTRW description of anomalous transport, is a conductivity histogram weighted by the particle flux. We show why this transition time pdf arises, and how to estimate the parameters of such probability distribution. The agreement between the simulations, pdf parameters, and fits to the resulting BTC is convincing.
- We develop a quantitative relationship between the key parameter in the transition time pdf, i.e., the power law exponent β, and the statistics of the underlying (correlated) hydraulic conductivity field.
- We identify the nature of transport (Fickian or anomalous) at a given observation scale by simply solving the flow field and using particle tracking to obtain a weighted particle visitation histogram. The computational effort is not unreasonable, and this point is critical for practical implications.
- We demonstrate that proposed models based on critical path analysis and percolation theory are not applicable. Significantly, the power law region of the transition times that controls the anomalous transport behavior lies below the critical path threshold.
- We highlight limitations of the oft-applied advection-dispersion equation showing that particle plume convergence to this model is not due to "homogenization" of the plume sampling in the domain, but rather to focusing of flow in a limited number of relatively uniform preferential pathways.

Finally, as noted in section 1, many geostatistical parameters and flow conditions are intimately linked, in terms of their effects on overall transport behavior. With the results presented here, which focused on specific parameter combinations, future studies will be directed to systematic and extensive analyses that consider, for a range of values of σ^2, variability in (i) correlation length, (ii) hydraulic gradient across the domain (also to more fully examine the role of diffusion and possible relevance of the Péclet number for characterization, and (iii) longer times (to further delineate the transition to Fickian behavior and the evolution of preferential pathways). Such analyses may facilitate further refinement of a quantitative relation between β and σ^2, and quantification of the $\mathcal{H}_w(K) \leftrightarrow \psi(t)$ relationship as a function of σ^2 and the transition to Fickian behavior.

Furthermore, in the above context, it should be recognized that the occurrence of preferential pathways has a major influence on reactive transport processes, where local variations in reactant concentrations lead to significant spatial variations in formation of the reaction products. The use of BTCs to establish parameters for conservative species, for example, in laboratory experiments, is in general not sufficient for analysis of a reactive transport system because such measurements do not provide detailed information on the flow patterns that determine the amount of reaction. This remains the subject of future investigations.

Appendix A: Correlations in the CTRW Framework

The essential feature of applying the CTRW to a diffusive or an advective-diffusive transport problem is the determination of the ensemble average of a form of the Master equation over realizations of the system.

The result of the ensemble average is $\psi(\mathbf{s}, t)$, the basic pdf governing the random walk. The ensemble average hence converts a transport problem in a heterogeneous system to one with statistical homogeneity, with a single density function $\psi(\mathbf{s}, t)$, i.e., it is a measure of the weighted full spectrum of all the local transitions in the system.

If the consistent result is a single pdf, then how can one account for correlations in the motion along a pathway, in which a transition depends on the previous one? The correlations must be introduced in each realization of the system and thus incorporated into the single $\psi(\mathbf{s}, t)$. Such a procedure can be followed with our model, where a correlation length ℓ is specified for the examined K-fields. The natural transition of particles in this system is based on the displacement and transit time associated with a change in velocity (due to a change in conductivity). An increase in ℓ tends to increase the displacement for a velocity change and can be accommodated in $\psi(\mathbf{s}, t)$, as will be shown in a future study.

We can explicitly relate the introduction of correlations in each realization to the subsequent ensemble average [*Curtin and Scher*, 1988]. We consider again the (above) model of a particle hopping among a random distribution of sites, which presents a clear model for anomalous diffusion. The transition rate $w(\mathbf{r}_n-\mathbf{r}_{n'})$ between sites depends only on the distance $\mathbf{r}_n-\mathbf{r}_{n'}$ between sites n, n'. The probability $P(\mathbf{r}_n, t)(\equiv P_n(t))$ that the particle is at site $\mathbf{r}_n$ can be determined by solution of the Master equation with initial condition $P_n(0)=\delta_{n,0}$:

$$\frac{dP_n(t)}{dt}=\sum_{n'\neq n} w_{nn'}P_{n'}(t)-\Gamma_n P_n(t), \tag{A1}$$

where $\Gamma_n=\sum_{n'\neq n} w_{n'n}$. The solution involves the inversion of a $N\times N$ matrix, where N is the total number of sites $(N\gg 1)$. We choose to limit the size of the matrix and consider a small finite cluster of sites. All of the transitions (back-and-forth) are retained as well, through Γ_n, representing the hops from each cluster site to all the other (background) sites in the system. This is called the cluster approximation. In this solution, the details of which are given in the following paragraph, one includes all the dynamics and correlations within the cluster, and yet the background remains as a sink.

The calculation of the probability $P(\mathbf{r}_n, t)(\equiv P_n(t))$ that a particle is at site $\mathbf{r}_n$ starts with solving the Master equation (with initial condition $P_n(0)=\delta_{n,0}$):

$$\frac{dP_n(t)}{dt}=\sum_{n'\neq n} w_{nn'}P_{n'}(t)-\Gamma_n P_n(t), \tag{A2}$$

where $\Gamma_n=\sum_{n'\neq n} w_{n'n}$. We simplify the notation $w(\mathbf{r}_n-\mathbf{r}_{n'})\equiv w_{nn'}$. Taking the Laplace transform of (A1), with $\mathcal{L}(P_n(t))=P_n(u)$ and adding $w_{nn}P_n(u)$ to both sides we obtain the matrix equation

$$P_n(u)=(u+\Gamma_n)^{-1}\sum_{n'} w_{nn'}P_{n'}(u)+(u+\Gamma_n)^{-1}\delta_{n,n_0}. \tag{A3}$$

The size of the matrix is $N\times N$, where N is the total number of sites $(N\gg 1)$. We apply a cluster approximation to the solution of (A3). In this solution, one includes all the dynamics and correlations within the cluster, and yet the background sites remains as a sink. We illustrate with the two-site cluster $1(=n_0), 2$: solve the matrix equation, expand the denominators, invert the Laplace transform, and sum the series to obtain

$$P_1(t)=\exp(-\Gamma_1 t)+\int_0^t d\tau \exp(-\Gamma_1\tau-\Gamma_2(t-\tau)) \times\left[\frac{w_{12}w_{21}\tau}{t-\tau}\right]^{\frac{1}{2}} I_1(\sigma), \tag{A4}$$

$$P_2(t)=\int_0^t d\tau \exp(-\Gamma_1\tau-\Gamma_2(t-\tau))w_{21}I_0(\sigma) \tag{A5}$$

where $\sigma\equiv[w_{12}w_{21}\tau(t-\tau)]^{\frac{1}{2}}$ and I_0, I_1 are modified Bessel functions of the first kind. The ensemble average of the time derivative of the first term of $P_1(t)$ is the η function [*Scher and Lax*, 1973]

mentioned above. The appearance of the Γ-functions, which contain all of the coupling to the background sites, in the exponentials, occurs for all size clusters. The exact ensemble average of the cluster forms are carried out in two stages, the first over the configuration of background sites and the next over the geometry within the cluster. The function $\langle\langle P_0(t)\rangle\rangle$ (simplified to $P_0(t)$) contains these two averages and is plotted in Figures 1 and 2 in *Curtin and Scher* [1988] in comparison to an exact simulation. These plots clearly show a systematic improvement with increasing compact cluster size.

Based on the above, the main result (Figures 1 and 2 in *Curtin and Scher* [1988]) shows $\langle P_0(t)\rangle$, for an exact ensemble average and for different cluster sizes, in comparison to an exact simulation. The size of the cluster modifies the time to remain on the initial site and improves the agreement with the exact simulation. The pdf $-\psi(t)$ is the time derivative of $\langle P_0(t)\rangle$ (see (11) in *Scher and Lax* [1973]). Hence, correlations in every realization of the system can be incorporated into the ensemble average determining the density function $\psi(t)$. The CTRW utilization of the cluster-size dependent $\psi(t)$ will be contained in a future study.

Appendix B: Equation (5) Derivation

The weighted histogram $\mathcal{H}_w(K)$ is interpreted by a probability density, which is then converted to time using $K^*=\theta\Delta x^2/(\Delta h^*\Delta t)$, with the understanding that the time associated with each K^* is the average transit time across a "K-bin."

The K values in Figure 3 can be plotted as

$$f=n_k\frac{\exp\left(-(\ln K-\mu)^2/2\sigma^2\right)}{t} \tag{B1}$$

where μ is the mean of $\mathcal{H}_w(K)$ and the variance of $\mathcal{H}_w(K)$ is $\approx\sigma^2$; n_k is a normalization constant.

We compute the logarithmic derivative of (B1), $d\log f/d\log t$. First, we have

$$\log f=\log n_k+\frac{-(\ln K-\mu)^2}{2\sigma^2}\log(e)-\log t. \tag{B2}$$

Then

$$d\log f/d\log t=\frac{(\ln K-\mu)}{\sigma^2}\log(e)\ln(10)-1 \tag{B3}$$

so that

$$d\log f/d\log t=\frac{(\ln K-\mu)}{\sigma^2}-1 \tag{B4}$$

because

$$\log(e)\ln(10)=1. \tag{B5}$$

The above is equated to $-1-\beta$, the log derivative of the truncated power law (2), in the power law region, to obtain (5) in the text.

The result in (5) has a slow time dependence for β, implicit in K (which is weighted by particle visitations, with times then determined by Darcy's law). In Figure 4, there is some curvature in the power law region. The value for β is determined near the end of the range of small ln (K) (large time).

Acknowledgments
The authors thank two anonymous reviewers and the Associate Editor for insightful and constructive comments. This research was supported (E. Y., B. B.) by the Israel Science Foundation (grant 221/11), and by the Israel Water Authority (grant 450056884). B. B. holds the Sam Zuckerberg Professorial Chair in Hydrology. Funding from MIUR (Italian Ministry of Education, Universities and Research—PRIN2010-11; project: "Innovative methods for water resources under hydro-climatic uncertainty scenarios") is acknowledged (A.G.).

References

Ababou, R., D. McLaughlin, L. W. Gelhar, and A. F. B. Tompson (1989), Numerical simulation of three-dimensional saturated flow in randomly heterogeneous porous media, *Transp. Porous Media*, *4*, 549–565.
Abramowitz, M., and I. Stegun (1970), *Handbook of Mathematical Functions*, Dover, New York.
Ambegaokar, V., B. I. Halperin, and J. S. Langer (1971), Hopping conductivity in disordered systems, *Phys. Rev. B*, *4*, 2612–2620.
Berkowitz, B., and H. Scher (1997), Anomalous transport in random fracture networks, *Phys. Rev. Lett.*, *79*(20), 4038–4041.
Berkowitz, B., and H. Scher (1998), Theory of anomalous chemical transport in fracture networks, *Phys. Rev. E*, *57*(5), 5858–5869.
Berkowitz, B., and H. Scher (2009), Exploring the nature of non-Fickian transport in laboratory experiments, *Adv. Water Resour.*, *32*, 750–755, doi:10.1016/j.advwatres.2008.05.004.
Berkowitz, B., and H. Scher (2010), Anomalous transport in correlated velocity fields, *Phys. Rev. E*, *81*, 011128, doi:10.1103/PhysRevE.81.011128.
Berkowitz, B., H. Scher, and S. E. Silliman (2000), Anomalous transport in laboratory-scale, heterogeneous porous media, *Water Resour. Res.*, *36*(1), 149–158.
Berkowitz, B., A. Cortis, M. Dentz, and H. Scher (2006), Modeling non-Fickian transport in geological formations as a continuous time random walk, *Rev. Geophys.*, *44*, RG2003, doi:10.1029/2005RG000178.
Berkowitz, B., S. Emmanuel, and H. Scher (2008), Non-Fickian transport and multiple-rate mass transfer in porous media, *Water Resour. Res.*, *44*, W03402, doi:10.1029/2007WR005906.
Bianchi, M., C. Zheng, C. Wilson, G. R. Tick, G. Liu, and S. M. Gorelick (2011), Spatial connectivity in a highly heterogeneous aquifer: From cores to preferential flow paths, *Water Resour. Res.*, *47*, W05524, doi:10.1029/2009WR008966.
Bijeljic, B., and M. J. Blunt (2006), Pore-scale modeling and continuous time random walk analysis of dispersion in porous media, *Water Resour. Res.*, *42*, W01202, doi:10.1029/2005WR004578.
Bijeljic, B., S. Rubin, H. Scher, and B. Berkowitz (2011), Non-Fickian transport in porous media with bimodal structural heterogeneity, *J. Contam. Hydrol.*, *120/121*, 213–221, doi:10.1016/j.jconhyd.2010.05.007.
Bijeljic, B., A. Raeini, P. Mostaghimi, and M. J. Blunt (2013a), Predictions of non-Fickian solute transport in different classes of porous media using direct simulation on pore-scale images, *Phys. Rev. E*, *87*, 013011, doi:10.1103/PhysRevE.87.013011.
Bijeljic, B., P. Mostaghimi, and M. J. Blunt (2013b), Insights into non-Fickian solute transport in carbonates, *Water Resour. Res.*, *49*, 2714–2728, doi:10.1002/wrcr.20238.
Bromly, M., and C. Hinz (2004), Non-Fickian transport in homogeneous unsaturated repacked sand, *Water Resour. Res.*, *40*, W07402, doi:10.1029/2003WR002579.
Ciriello, V., A. Guadagnini, V. Di Federico, Y. Edery, and B. Berkowitz (2013), Comparative analysis of formulations for conservative transport in porous media through sensitivity-based parameter calibration, *49*, 5206–5220, doi:10.1002/wrcr.20395.
Cirpka, O. A., and P. K. Kitanidis (2000), Characterization of mixing and dilution in heterogeneous aquifers by means of local temporal moments, *Water Resour. Res.*, *36*(5), 1221–1236, doi:10.1016/j.jconhyd.2012.02.005.
Cirpka, O. A., and C. J. Surabhin (2004), Measurements of mixing-controlled reactive transport in homogeneous porous media and its prediction from conservative tracer test data, *Environ. Sci. Technol.*, *38*(7), 2089–2096.
Cordes, C., and W. Kinzelbach (1992), Continuous groundwater velocity fields and path lines in linear, bilinear, and trilinear finite elements, *Water Resour. Res.*, *28*(11), 2903–2911.
Cortis, A., and B. Berkowitz (2005), Computing "anomalous" contaminant transport in porous media: The CTRW Matlab toolbox, *Ground Water*, *43*(6), 947–950.
Cortis, A., Y. Chen, H. Scher, and B. Berkowitz (2004), Quantitative characterization of pore-scale disorder effects on transport in "homogeneous" granular media, *Phys. Rev. E*, *70*(4), 041108, doi:10.1103/PhysRevE.70.041108.
Curtin, W. A., and H. Scher (1988), Hopping transport in disordered systems: Correlation effects, *Mater. Res. Soc. Proc.*, *135*, 89–94, doi:10.1557/PROC-135-89.
Cushman, J. H., and T. R. Ginn (1993), Nonlocal dispersion in media with continuously evolving scales of heterogeneity, *Transp. Porous Media*, *13*(1), 123–138.
Dagan, G., and S. P. Neuman (1997), *Subsurface Flow and Transport: A Stochastic Approach*, Cambridge Univ. Press, Cambridge, U. K.
Di Donato, G., and M. J. Blunt (2004), Streamline-based dual-porosity simulation of reactive transport and flow in fractured reservoirs, *Water Resour. Res.*, *40*, W04203, doi:10.1029/2003WR002772.
Domenico, P. A., and F. W. Schwartz (1990), *Physical and Chemical Hydrogeology*, John Wiley, New York.
Fiori, A., and I. Jankovic (2012), On preferential flow, channeling and connectivity in heterogeneous porous formations, *Math. Geosci.*, *44*, 133–145, doi:10.1007/s11004-011-9365-2.
Fogg, G. E. (2010), Log-K variance, connectivity, unconformities and non-Fickian transport, *Geol. Soc. Am. Abstr. Programs*, *42*, 42.
Ghanbarian-Alavijeh, B., T. E. Skinner, and A. G. Hunt (2012), Saturation dependence of dispersion in porous media, *Phys. Rev. E*, *86*, 066316.
Gómez-Hernández, J. J., and A. G. Journel (1993), Joint sequential simulation of multi-Gaussian field, in *Geostatitics Troia'92*, vol. 1, edited by A. Soares, pp. 85–94, Kluwer Acad., Dordrecht, Netherlands.
Guadagnini, A., and S. P. Neuman (1999), Nonlocal and localized analyses of conditional mean steady state flow in bounded, randomly nonuniform domains, 1, theory and computational approach, *Water Resour. Res.*, *35*, 2999–3018.
Haggerty, R., S. A. McKenna, and L. C. Meigs (2000), On the late-time behavior of tracer test breakthrough curves, *Water Resour. Res.*, *36*(12), 3467–3479.
Hunt, A. G., T. E. Skinner, R. P. Ewing, and B. Ghanbarian-Alavijeh (2011), Dispersion of solutes in porous media, *Eur. Phys. J. B*, *80*, 411–432, doi:10.1140/epjb/e2011-10805-y.
Huysmans, M., and A. Dassargues (2009), Application of multiple-point geostatistics on modelling groundwater flow and transport in a cross-bedded aquifer (Belgium), *Hydrogeol. J.*, *17*, 1901–1911.
Kang, P. K., M. Dentz, T. Le Borgne, and R. Juanes (2011), Spatial Markov model of anomalous transport through random lattice networks, *Phys. Rev. Lett.*, *107*, 180602.
Kirkpatrick, S. (1971), Classical transport in disordered media: Scaling and effective-medium theories, *Phys. Rev. Lett.*, *27*, 1722–1725.
Knudby, C., and J. Carrera (2005), On the relationship between geostatistical, flow and transport connectivity measures, *Adv. Water Resour.*, *28*, 405–421.
Kosakowski, G. (2004), Anomalous transport of colloids and solutes in a shear zone, *J. Contam. Hydrol.*, *72*(1–4), 23–46, doi:10.1016/j.jconhyd.2003.10.005.

Kosakowski, G., B. Berkowitz, and H. Scher (2001), Analysis of field observations of tracer transport in a fractured till, *J. Contam. Hydrol.*, *47*(1), 29–51.
Kuntz, B. W., S. Rubin, B. Berkowitz, and K. Singha (2011), Quantifying solute transport at the Shale Hills critical zone observatory, *Vadose Zone J.*, *10*, 843–857, doi:10.2136/vzj2010.0130.
Le Borgne, T., M. Dentz, and J. Carrera (2008), Spatial Markov processes for modeling Lagrangian particle dynamics in heterogeneous porous media, *Phys. Rev. E*, *78*, 026308.
Levy, M., and B. Berkowitz (2003), Measurement and analysis of non-Fickian dispersion in heterogeneous porous media, *J. Contam. Hydrol.*, *64*, 203–226.
Llopis-Albert, C., and J. E. Capilla (2009), Gradual conditioning of non-Gaussian transmissivity fields to flow and mass transport data: 3. Application to the Macrodispersion Experiment (MADE-2) site, on Columbus Air Force Base in Mississippi (USA), *J. Hydrol.*, *371*, 75–84.
Margolin, G., and B. Berkowitz (2002), Spatial behavior of anomalous transport, *Phys. Rev. E*, *65*, 031101, doi:10.1103/PhysRevE.65.031101.
Mariethoz, G., and P. Renard (2010), Reconstruction of incomplete data sets or images using direct sampling, *Math. Geosci.*, *42*, 245–268.
Mettier, R., G. Kosakowski, and O. Kolditz (2006), Influence of small-scale heterogeneities on contaminant transport in fractured crystalline rock, *Ground Water*, *44*(5), 687–696.
Montroll, E. W., and H. Scher (1973), Random walks on lattices. IV. Continuous-time walks and influence of absorbing boundaries, *J. Stat. Phys.*, *9*(2), 101–135.
Morales Casique, E., S. P. Neuman, and A. Guadagnini (2006a), Nonlocal and localized analyses of nonreactive solute transport in bounded randomly heterogeneous porous media: Theoretical framework, *Adv. Water Resour.*, *29*, 1238–1255.
Morales Casique, E., S. P. Neuman, and A. Guadagnini (2006b), Nonlocal and localized analyses of nonreactive solute transport in bounded randomly heterogeneous porous media: Computational analysis, *Adv. Water Resour.*, *29*, 1399–1418.
Moroni, M., and J. H. Cushman (2010), Three-dimensional particle tracking velocimetry studies of the transition from pore dispersion to Fickian dispersion for homogeneous porous media, *Water Resour. Res.*, *37*, 873–884, doi:10.1029/2000WR900364.
Panzeri, M., M. Riva, A. Guadagnini, and S. P. Neuman (2013), Data assimilation and parameter estimation via ensemble Kalman filter coupled with stochastic moment equations of transient groundwater flow, *Water Resour. Res.*, *49*, 1334–1344, doi:10.1002/wrcr.20113.
Pfister, G., and H. Scher (1978), Non-Gaussian transient transport in disordered solids, *Adv. Phys.*, *27*, 747–798.
Riva, M., A. Guadagnini, D. Fernandez-Garcia, X. Sanchez-Vila, and T. Ptak (2008), Relative importance of geostatistical and transport models in describing heavily tailed breakthrough curves at the Lauswiesen site, *J. Contam. Hydrol.*, *101*, 1–13.
Riva, M., A. Guadagnini, and X. Sanchez-Vila (2009), Effect of sorption heterogeneity on moments of solute residence time in convergent flows, *Math. Geosci.*, *41*, 835–853, doi:10.1007/s11004-009-9240-6.
Riva, M., L. Guadagnini, and A. Guadagnini (2010), Effects of uncertainty of lithofacies, conductivity and porosity distributions on stochastic interpretations of a field scale tracer test, *Stochastic. Environ. Res. Risk Assess.*, *24*, 955–970, doi:10.1007/s00477-010-0399-7.
Rubin, S., I. Dror, and B. Berkowitz (2012), Experimental and modeling analysis of coupled non-Fickian transport and sorption in natural soils, *J. Contam. Hydrol.*, *132*, 28–36, doi:10.1016/j.jconhyd.2012.02.005.
Rubin, Y. (2003), *Applied Stochastic Hydrology*, Oxford Univ. Press, New York.
Sahimi, M. (2012), Dispersion in porous media, continuous-time random walks, and percolation, *Phys. Rev. E*, *85*, 016316.
Salamon, P., D. Fernandez-Garcia, and J. Gomez-Hernandez (2007), Modeling tracer transport at the MADE site: The importance of heterogeneity, *Water Resour. Res.*, *43*, W08404, doi:10.1029/2006WR005522.
Sanchez-Vila, X., and J. Carrera (2004), On the striking similarity between the moments of breakthrough curves for a heterogeneous medium and a homogeneous medium with a matrix diffusion term, *294*(1–3), 164–175.
Sanchez-Vila, X., A. Guadagnini, and J. Carrera (2006), Representative hydraulic conductivities in saturated groundwater flow, *Rev. Geophys.*, *44*, RG3002, doi:10.1029/2005RG000169.
Scher, H., and M. Lax (1973), Stochastic transport in a disordered solid. II. Impurity conduction, *Phys. Rev. B*, *7*(1), 4502–4519.
Scher, H., M. F. Shlesinger, and J. T. Bendler (1991), Time-scale invariance in transport and relaxation, *Phys. Today*, *26–34*.
Strebelle, S. (2002), Conditional simulation of complex geological structures using multiple-point geostatistics, *Math. Geol.*, *34*, 1–21.
Tartakovsky, D. M., and S. P. Neuman (1998), Transient flow in bounded randomly heterogeneous domains 1. Exact conditional moment equations and recursive approximations, *Water Resour. Res.*, *34*(1), 1–12.
Willmann, M., J. Carrera, and X. Sánchez-Vila (2008), Transport upscaling in heterogeneous aquifers: What physical parameters control memory functions?, *Water Resour. Res.*, *44*, W12437, doi:10.1029/2007WR006531.
Zinn, B., and C. F. Harvey (2003), When good statistical models of aquifer heterogeneity go bad: A comparison of flow, dispersion, and mass transfer in connected and multivariate Gaussian hydraulic conductivity fields, *Water Resour. Res.*, *39*(3), 1051, doi:10.1029/2001WR001146.